



# Intensive Studies for Modeling and Thermodynamics of Fusion Digestion Processes of Abu Rusheid Mylonite Rocks

AHMED A. ELIWA,<sup>1</sup> EBRAHIM A. GAWAD,<sup>1</sup> AMAL E. MUBARK,<sup>1,2</sup>  
and NASR A. ABDELFAH<sup>1</sup>

1.—Nuclear Materials Authority, El Maadi, P.O. Box 530, Cairo, Egypt.  
2.—e-mail: amal\_mubark2014@yahoo.com

Mylonite rocks of the Abu Rusheid area, Southeastern Desert of Egypt, were physically upgraded producing Zr, Ti, Nb, and REEs concentrate. Comparative fusion digestion studies of the concentrate using NaOH and KOH were carried out. Dissolution efficiencies of 83.4%, 99.8%, 69.7%, and 97.1% for Zr, Nb, Ti, and REEs, respectively, were accomplished using NaOH under 1023 K, 90 min, 1:1.25 ratio, and 74  $\mu\text{m}$  particle size. However, 79.5, 87.3, 90.5, and 97.4% were achieved using KOH under 1023 K, 90 min, 1:1.75 ratio, and 44  $\mu\text{m}$  particle size. Suggested pseudo-reversible first-order, uptake general, and shrinking core models fitted well with the experimental results using the two alkalis. Convergent activation energies were calculated using the three models. A suggested Floatotherm including the Van't Hoff parameters model showed endothermic and spontaneous behavior with a decrease in the randomness at the solid/solution interface during the attack of fused alkali on the concentrate particles.

## INTRODUCTION

The Abu Rusheid area, Southeastern Desert of Egypt, is one of the most important areas, especially for rare-metal mineralization. It is located about 97 km southwest of Marsa Alam city between longitudes 34°46'–34°46'35"E and latitudes 24°37'16"–24°38'N. The area can be reached from the Red Sea coast through Wadi El Gemal and then Wadi Nugrus along a desert track about 40 km long.<sup>1</sup>

The potentialities for mineralizations in the Abu Rusheid area and its surroundings have been discussed in various works.<sup>2–4</sup> The study area is characterized by low to moderate topography. According to Ibrahim et al.,<sup>2</sup> the sequence of the Precambrian rocks in the Abu Rusheid area are: (1) ophiolitic mélangé, consisting of ultramafic rocks and layered metagabbros with a metasedimentary matrix, (2) cataclastic rocks (peralkalic granitic gneisses) in the core of the granitic pluton, which are composed of protomylonites, mylonites, ultramylonites, and silicified ultramylonites, (3) mylonitic granites, and (4) post-granitic dykes and veins.<sup>5</sup>

The Abu Rusheid area is a distinctive occurrence of economically important rare-metal mineralization where the host rocks are represented by granitic gneisses. The shear zones' rare-metal minerals, identified from the peralkalic granitic gneisses and cataclastic to mylonitic rocks, are associated with muscovite, chlorite, quartz, fluorite, pyrite, magnetite, and rare biotite.<sup>6</sup> Several minerals have been identified, namely: (1) Columbite-Tantalite, Pyrochlore, Ferrocolumbite, and Cassiterite minerals, (2) Zircon, (3) Rutile, and high-Ti Pyrochlore, and (4) Cheralite, Monazite, and Xenotime.<sup>7–10</sup>

Zirconium, titanium, niobium, and rare-earth elements (REEs), with high melting points, have been utilized widely in almost all walks of life. The extraction of these metals from their ores has been studied for many years, and a large number of procedures have been reported. Their minerals, which occur in the form of multiple oxides, are commonly refined by different methods, including acid leaching, pressure leaching, acid roasting, and chloride roasting.<sup>11–17</sup> Owing to the refractory nature of these minerals,<sup>18</sup> and their resistance to acid attack in moderate conditions, more aggressive conditions are required for leaching than those used

in conventional circuits. Among these methods, alkali fusion was the first to be industrially applied. Fusion digestion techniques of refractory minerals from their ores have been investigated successfully using different fluxes, namely potassium hydrogen sulfate, sodium pyrosulfate, potassium hydrogen fluoride, potassium pyrosulfate, sodium carbonate and sugar charcoal, and borax. Alkali hydroxides have been widely tested for the fusion dissolution of the studied minerals and have proved effective in the digestion process.<sup>19–23</sup> Recently, a new process for the leaching of low-grade refractory ores with KOH sub-molten salt has been proposed to eliminate fluorine pollution at the source, and to obtain a cleaner production process, to achieve optimum resource utilization.<sup>20,24</sup>

Flux fusion is often used as an alternative to acid dissolution. This dissolution method is often used for the dissolution of samples such as mineral ores, slags, and some metal oxides which are resistant to acid attack. The sample is converted into a form that is soluble in acids, bases, or water due to a combination of oxidation and acid/base reactions that take place between the flux and the inorganic sample. The dissolution of the sample is normally dependent on the sample: flux weight ratio as well as the melting point of the flux salt. When the reaction is complete, judged by visual inspection which is indicated by the disappearance of all the starting material, the melt is allowed to cool and then dissolved in acid, base, or water.

Conceived predictive diagonal (CPD) is a trial technique for achieving workable and accurate results via innovative easy and time-saving methodologies. The goal of the CPD technique is to carry out fewer experiments and obtain a more professional analysis. This technique does not depend on the matrix diagonally dominant techniques or the eigenvalue principle, while, at the same time, it differs from design of experiment and Taguchi techniques.<sup>25</sup>

The CPD technique supposes that, if the distribution of the factors covers the task range skillfully in sequence to obtain the homogenous response, the diagonal of the conceived predictive matrix is enough to represent this case. The study depends on re-modeling two factors simultaneously to achieve applicable accurate results, and is considered as an important step within a great achievement. Thus, if the process goes without obstacles, the other points will be canceled and the saved time can be employed to study another pairs of factors simultaneously. This type of technique needs skills in matrices, nonlinear regression modeling, MATLAB, and kinetics–thermodynamics relationships. For prospective proceeding, the simulated models can be optimized using MATLAB or any available software.<sup>26–28</sup>

In our study, fluxing digestion of Egyptian Mylonite concentrates, which contained Zr, Ti, Nb, and REEs and were obtained from the Abu Rushied

area, was carried out using sodium and potassium hydroxide fluxes separately. The digestion experiments were achieved using the CPD technique through two groups of experiments. The first group was studied by variation of time and temperature simultaneously under a fixed ore to alkali ratio and the ore mesh size digestion conditions. The second group was performed by the variation of the ore to alkali ratio and the ore mesh size simultaneously under fixed digestion time and temperature processes. To improve the recovery processes of the Zr, Ti, Nb, and REEs using alkali flux digestion, three kinetic models were studied using the experimental digestion results. The MATLAB mathematical results, which were obtained from the three models, were utilized to determine the activation energy, kinetics, thermodynamics, and the empirical model equation for each dissolution process.

The main aims of the fusion digestion study of Mylonite rocks were:

- Reducing the time required for dissolution of titanium minerals which are presented mainly in the Abu Rusheid Mylonite concentrate, decrease the concentration of the fluxing agent, and diminish the energy necessary for performing the fusion process. These minerals consume high energies, high temperatures, and long digestion times using sodium and potassium hydroxide fluxes.<sup>29–32</sup>
- Choosing the most appropriate fluxing conditions for the other elements (Zr, Nb, and REEs), in terms of fluxing time, temperature, and the amount of energy consumed in the melting process.
- Studying the kinetics–thermodynamics relationships for Zr, Nb, Ti, and REEs dissolution using several models. These was carried out to determine the rate laws governing the dissolution and to determine the activation energy, kinetics, and thermodynamics for each dissolution process using the two fluxes.

## EXPERIMENTAL

### Materials and Reagents

All the chemicals used in the experimental work were analytical grade, including potassium hydroxide pellets (KOH) (99%; Prolabo), sodium hydroxide pellets (NaOH) (99%; Prolabo), hydrochloric acid (HCl) (37%; Fluka), and bromoform (CHBr<sub>3</sub>) (99%; Merck). All the chemicals were used as received. The Mylonite rocks sample under study was collected from the Abu Rushied area and was subjected to a physical pre-concentration (upgrading) process by shaking table to remove undesirable associated minerals. A representative upgraded concentrate was first dried at 110°C for 24 h, ground to the proper mesh size, then subjected to analysis by x-ray fluorescence analysis at the Analytical Lab in

the Egyptian Atomic Power Agency (a PHILIPS X'UNIQUE II spectrometer Rh-target tube, 70 KV, 15 mA, LiF-220 analyzing crystal, and a Rh-target tube, 30 KV, 60 mA, PE-001 analyzing crystal) to determine the components present in the concentrates.

To study the mineralogical composition of the concentrate sample, heavy mineral separation procedures were applied. The concentrate sample was ground to -60 mesh size to liberate the heavy minerals, and then washed with distilled H<sub>2</sub>O. The heavy fractions were separated from the different sizes by bromoform, and the heavy mineral grains were picked under a binocular microscope from each of the obtained heavy fractions. Mineralogical analysis of the bulk concentrate sample before and after fusion process was carried out by x-ray diffraction analysis (Philips PW 223/30). A scanning electron microscope (SEM) was used to identify the mineral grains. The SEM was equipped with an energy dispersive spectrometer (EDS) unit (Philips XL 30). The measurement conditions were an accelerating voltage of 30 kV with a beam diameter of 1 mm for a counting time of 60–120 s, and a minimum detectable weight concentration ranging from 0.1 to 1 wt. %.

### Alkali Fusion Process

Several experiments were performed by mixing a constant weight (5 g) of the fine ground concentrate sample with solid KOH and NaOH, each separately, as the fused reagent. Different factors affecting the dissolution of the Zr, Ti, Nb, and REEs from the Mylonite concentrate were studied and are summarized in Table I, namely; contact time, reaction temperature, ore grain size, and ore/alkali ratios.

The experiments were carried out under the following fixed conditions:

- To obtain professional data with fewer experiments, the CPD technique was suggested for this target. The CPD is a useful technique that helped us to understand the complicated sub-systems easily. It was achieved through studying two factors simultaneously.
- The 12 fusion experiments were conducted using the two hydroxides separately, which means a 24-melting process was carried out using the

conditions as mentioned in Table I.

- The two phases, ground ore concentrate and alkali, were mixed in a platinum crucible under the variable parameters before the fluxing process.
- After each experiment, the retained crucible was allowed to cool to ambient temperature then subjected to acid dissolution using 6 M hydrochloric acid under a leaching temperature of 363 K for 30 min. The leaching processes were conducted using a 250-ml flask and stirred with 500 rpm agitating speed by a hot plate magnetic stirrer.
- The pregnant chloride leach liquor was filtered out using filter paper (Whatman 41) and analyzed for determining their Zr, Ti, Nb, and REEs content using inductively coupled plasma–optical emission spectrometry (Agilent Technologies).
- Double variable testing was used for the optimization of the fusion parameters. In this approach, a series of fusion tests using the two alkalis were performed by changing the two variables together and maintaining the other variables at fixed values for a given set of measurements.

## RESULTS AND DISCUSSION

### Ore Characterization

A representative pre-concentrated sample from the Mylonite rocks of the Abu Rusheid area was analyzed using x-ray fluorescence analysis. The obtained results (Fig. 1a) revealed a high concentration of Zr, Ti, Nb, and REEs. These elements were presented in the refractory minerals.

The bulk concentrate sample was characterized using XRD analysis to identify the present mineralizations, as shown in Fig. 1b, revealing the presence of Zircon, Titanite, and Albite as the main components. For mineral identification, separated mineral grains were characterized using SEM-EDX analysis, as shown in Fig. 2, which revealed the presence of valuable minerals such as Monazite [(Ce,La,Nd,Th)PO<sub>4</sub>.SiO<sub>4</sub>], Zircon (ZrSiO<sub>4</sub>), Columbite [(Fe,Mn)(Nb,Ta)<sub>2</sub>O<sub>6</sub>], and Titanite [CaTiSiO<sub>5</sub>]. The presence of these minerals together reflected

**Table I. Studied fusion experiments**

Exp. No.	Temp., K	Time, min.	Ore size, $\mu\text{m}$	Ore :alkali ratio, w/w	Exp. No.	Temp., K	Time, min.	Ore size, $\mu\text{m}$	Ore /alkali ratio, w/w
1	873	45	74	1:1.5	7	1023	90	74	1:1
2	923	60	74	1:1.5	8	1023	90	74	1:1.25
3	973	75	74	1:1.5	9	1023	90	63	1:1.5
4	1023	90	74	1:1.5	10	1023	90	63	1:1.75
5	1073	105	74	1:1.5	11	1023	90	44	1:2
6	1123	120	74	1:1.5	12	1023	90	44	1:2.25

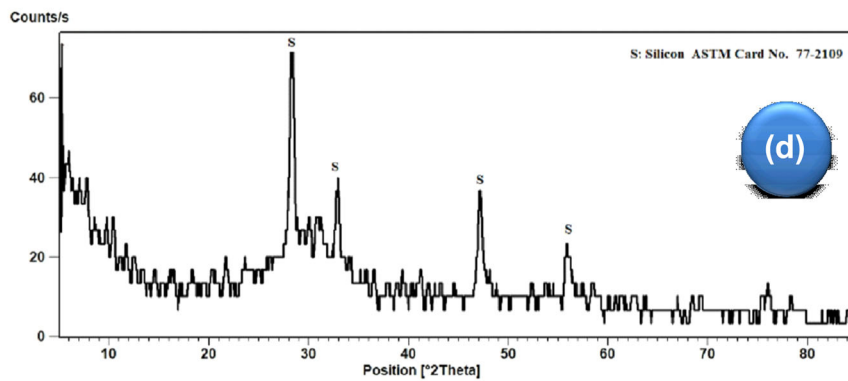
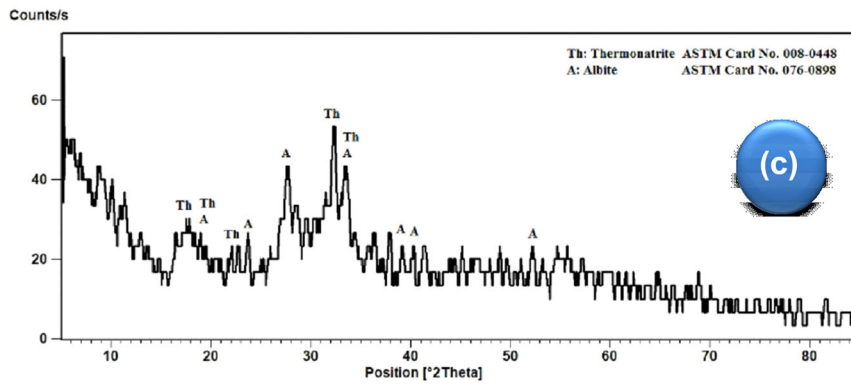
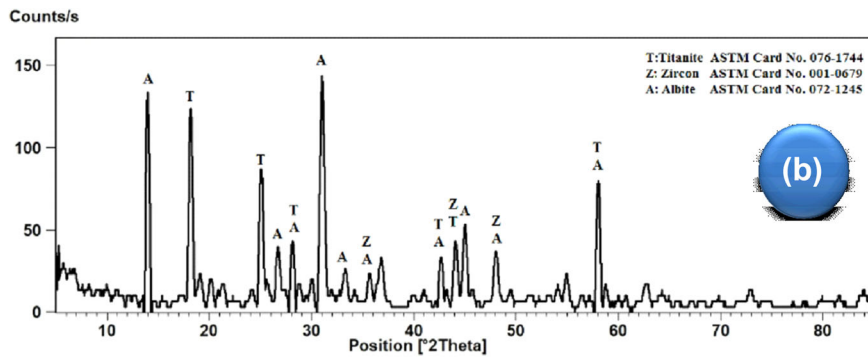
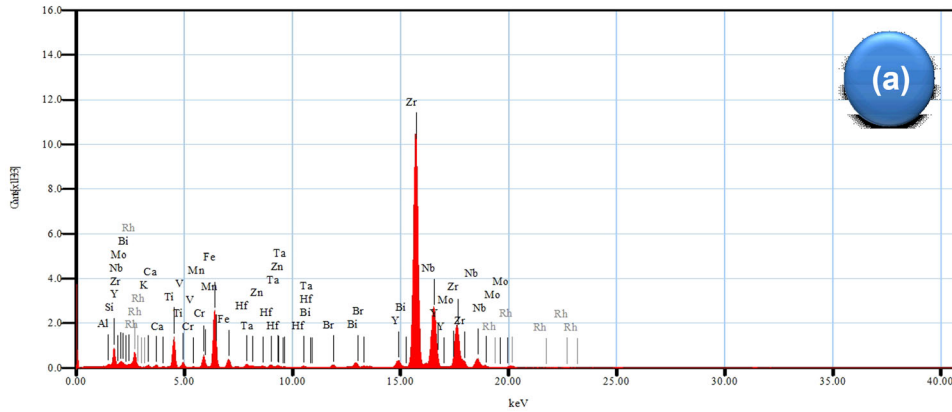


Fig. 1. (a) XRF-chart for the Mylonite concentrates Abu Rushied area (b) XRD chart for the bulk concentrates sample (c) After NaOH fusion and (d) After KOH fusion.



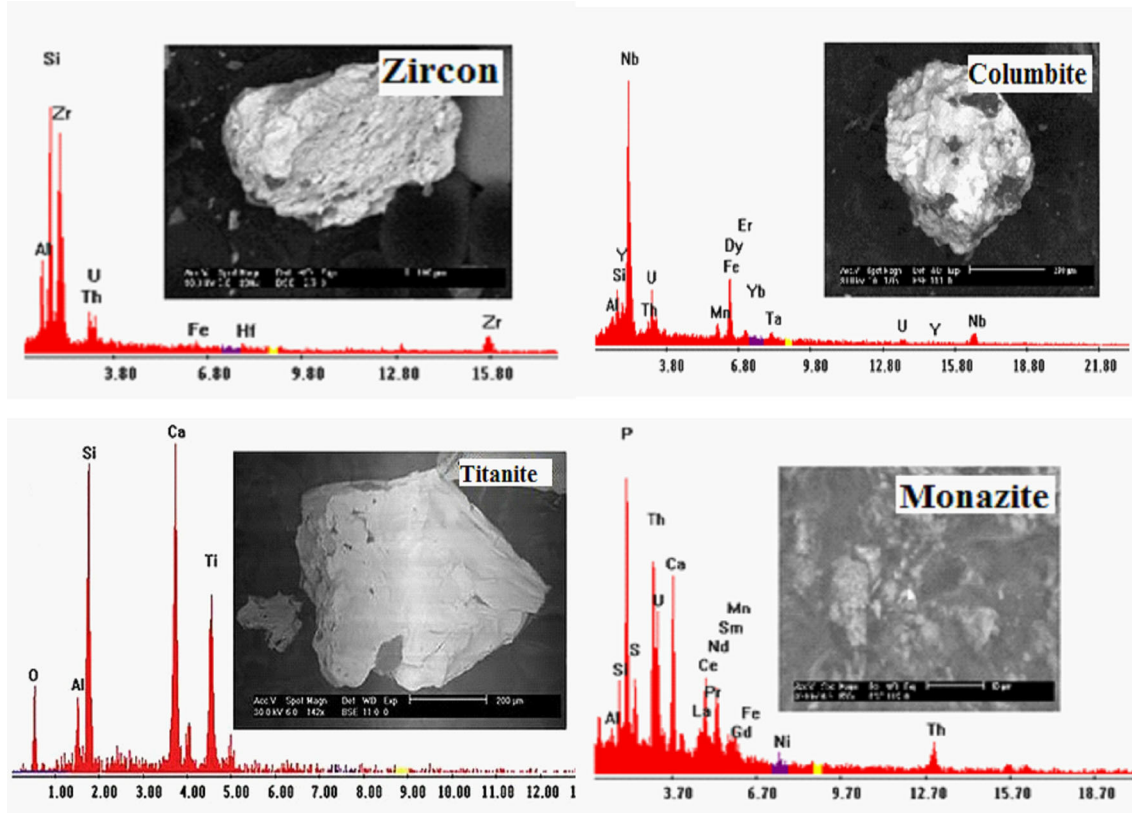


Fig. 2. SEM-EDAX pattern of separated grains.

the refractory nature of this concentrate sample during processing.

### Fusion Digestion Process of the Concentrate Sample

Four factors were studied on the dissolution of the Zr, Ti, Nb, and REEs content from the concentrate sample using sodium and potassium hydroxides in two groups. By changing the time with the temperature of the fusion processes under a fixed ore to alkali ratio and ore particle size, 12 experiments using the two alkalis were considered the first group. On the other hand, another 12 experiments were conducted under the variation of both the ore to alkali ratio and the ore particle size with fixed time and temperature of the fusion processes, which was considered the second group.

From the results illustrated in Fig. 3, it can be concluded that:

- Generally, by increasing the fusion time from 45 to 90 min and enhancing the temperature from 873 to 1023 K, the leaching efficiency of Zr, Ti, Nb, and REEs increased sharply. However, by increasing the time and temperature over 90 min and 1023 K, respectively, there were very small improvements in the dissolution of the titanium and niobium elements, while there was a reduction in zirconium dissolution. Ti and Nb miner-

als, which were present in the concentrate, achieve high temperatures using sodium and potassium hydroxide fluxes (over 1073 K).<sup>29–33</sup>

On the other hand, Zr, which was present in the concentrate, consumed lower temperatures than the Ti and Nb minerals (from 873 to 923 K).<sup>34,35</sup>

- Thus, 90 min and 1023 K as the fusion time and temperature were considered the more confident values for the two studied parameters to be applied in the second group.
- In the second group, the ore to alkali ratio played an important role in the dissolution of all the studied elements. It was noticed that the solid to alkali ratio of 1:1.25, and the 74- $\mu\text{m}$  concentrate particle size were the more appropriate conditions in which 83.4, 99.8, 69.7, and 97.1% leaching efficiency for Zr, Nb, Ti, and REEs, respectively, was achieved by using sodium hydroxide as a flux. In the potassium hydroxide experiments, a solid to alkali ratio of 1:1.75 and 44- $\mu\text{m}$  concentrate particle size were the proper choice, resulting in 79.6, 87.3, 90.5, and 97.4% dissolution efficiency for Zr, Nb, Ti, and REEs, respectively.
- Sodium hydroxide as a flux was more distinct than potassium hydroxide in the leaching of Nb and Zr. However, potassium hydroxide was preferred in the dissolution of Ti. For the REEs, both refluxes gave the maximum dissolution efficiency.

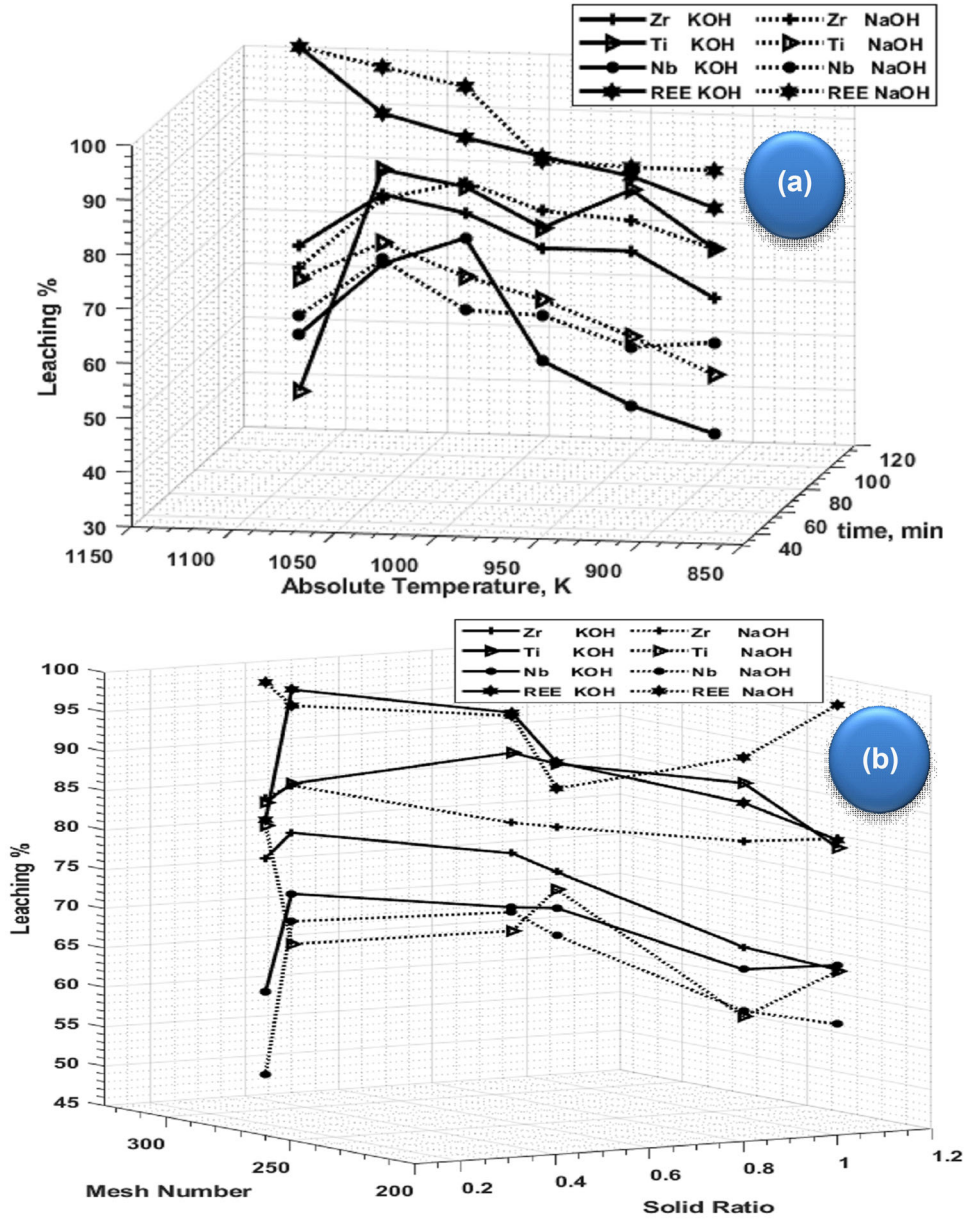


Fig. 3. (a) Time and temperatures (b) solid ratio mesh size dissolution 3D curves for Zr, Ti, Nb and REEs using sodium and potassium hydroxides.

- XRD analysis of the Mylonite concentrate indicated a significant presence of tantalite and zircon minerals, and in higher concentrations than other desired minerals such as columbite and monazite (Fig. 1b). XRD analysis of the leaching residues after the NaOH and KOH fusion processes indicated that silicon was the main residual obtained (Fig. 1c and d).

**Dissolution Kinetics**

Several models were investigated to explain the chemical reaction and to determine the order of the dissolution reaction.

*Pseudo First-Order General Model*

The first step in understanding how a given chemical reaction occurs is to determine the form of the rate law. The general model was generated by Eqs. 1 and 2.

For the concentration relationship pseudo-first-order reaction (Eq. 1):<sup>36</sup>

$$C = (C_o - C_e) \exp(-Kt) \tag{1}$$

where  $C$ ,  $C_o$ , and  $C_e$  are the dissolved element concentrations at any time  $t$ , the initial concentration of the studied elements, and their concentration at equilibrium, respectively, and  $k$  is the reaction rate constant,

And from the Arrhenius relationship (Eq. 2):<sup>37</sup>

$$K = Ar \exp(E/RT) \quad (2)$$

where  $T$  is the absolute temperature in kelvins,  $Ar$  is the Arrhenius constant,  $E$  is the activation energy for the reaction, and  $R$  is the universal gas constant.

By introducing Eq. 1 into Eq. 2, for an irreversible reaction:

$$C = (C_o - C_e) \exp(-t Ar \exp(E/RT)) \quad (3)$$

However, for a reversible (or parallel) reaction:

$$C = a C_o \exp(-t Ar_1 \exp(E_1/RT)) + (C_o - a) \exp(-t Ar_2 \exp(E_2/RT)) \quad (4)$$

where  $Ar_1$ ,  $Ar_2$ ,  $E_1$ , and  $E_2$  are the Arrhenius constants and activation energy for the two parallel reactions, respectively. The reversible or parallel reactions are determined from the sign of the reaction rate constants for the two reactions. When they have the same sign, the two reactions are parallel, while having an opposite sign indicates the reversibility of the reactions.

By applying the suggested general model (Eq. 4) (pseudo-reversible first-order) using the results of the dissolution processes at several temperatures and times (Group 1) for Nb, Zr, Ti, and REEs, the experimental results have been graphed using the MATLAB program in 3D curves, as shown in Fig. 4a and S7A (see supplementary data file). The activation energies and correlation coefficients for the dissolution reactions using the two alkalis for Nb, Zr, Ti, and REEs are shown in Table II.

The obtained figures show that the dissolution reactions of Zr, Nb, Ti, and REEs using sodium and potassium hydroxides matched well with the suggested pseudo-first-order model, and high correlation coefficients,  $R^2$ , were obtained for most of the dissolution processes shown in Table II.

From the results, it was indicated that the rare-earth dissolution process was carried out through one reaction (irreversible) with convergent activation energy using the two alkalis. On the other hand, the Zr, Nb, and Ti dissolution processes were accomplished through two reactions with two variable activation energies, one of them having a much higher value than the other.

The fusion digestion of the Zr, Nb, REEs, and Ti of the Mylonite concentrate using sodium or potassium hydroxides as a flux needed activation energies in the range of 31–38 kJ/mol. Different from the others, The Nb dissolution using potassium hydroxide needed only 16.1 kJ/mol.

On the other hand, another relationship for the pseudo-first-order reaction was used to explain the dissolution processes obtained from the group 2 experimental data (by variation of both the ore to alkali ratio and the ore particle size with fixed time and temperature).

For the concentration relationship pseudo-first-order;

$$C_{(r)} = C_o \exp(K_1 r) \quad (5)$$

$$C_{(M)} = C_o \exp(K_2 M) \quad (6)$$

where  $C_{(r)}$ ,  $C_{(M)}$ , and  $C_o$  are the dissolved element concentrations at any ore to alkali ratio, the ore particle size, and the initial concentration of the studied elements, respectively.  $K_1$  and  $K_2$  are the reaction rate constants.

From Eqs. 5 and 6;

$$C_{(r,M)} = C_o \exp(k_1 r + K_2 M) \quad (7)$$

where  $C_{(r,M)}$  is the dissolved element concentration related to both the ore to alkali ratio and the ore particle size.

By applying the suggested general model (Eq. 7) (pseudo-reversible first-order), using the results of the dissolution processes at different ore to alkali ratios and the ore particle sizes (Group 2) for Nb, Zr, Ti, and REEs, the experimental results have been graphed using MATLAB program in three dimensions 3D curves as shown in Figs. 4b and S7B (see supplementary data file). The obtained figures show that the dissolution reaction of Zr, Nb, Ti, and REEs using sodium and potassium hydroxides matched well with the suggested pseudo-first-order model, and a high correlation coefficient  $R^2$  was obtained for most of the dissolution processes. It was seen that there was a noticeable difference in the dissolution reaction of Zr, Nb, Ti, and REEs using sodium and potassium hydroxides. It was also found that  $K_1$  and  $K_2$  have the same sign in the case of using sodium peroxide as a flux, while, in the case of using potassium peroxide, they have opposite signs. As a result, the dissolution reaction in the sodium hydroxide case was carried out through a parallel reaction, while in the other case it was carried out through a reversible reaction.

#### Uptake General Model

The dissolution results of Zr, Nb, Ti, and REEs of Mylonite concentrate using sodium or potassium hydroxides as fluxes were represented with the uptake general model. The uptake general model (Eq. 11) was derived as follows:<sup>25</sup>

The pseudo- $n$ th-order rate equation (Eq. 8) which can be derived as follows for any pseudo- $n$  order:<sup>37</sup>

$$dq/dt = k(q_e - q_t)^n \quad (8)$$

where  $q_e$ ,  $q_t$ , and  $n$  are the dissolved element concentrations at equilibrium  $t$ , their concentration at any time, and order of reaction, respectively.

By separation and integration, we obtain:

$$q_t = q_e - \left( q_e^{(1-n)} + (k(n-1)t) \right)^{(1-(1-n))} \quad (9)$$



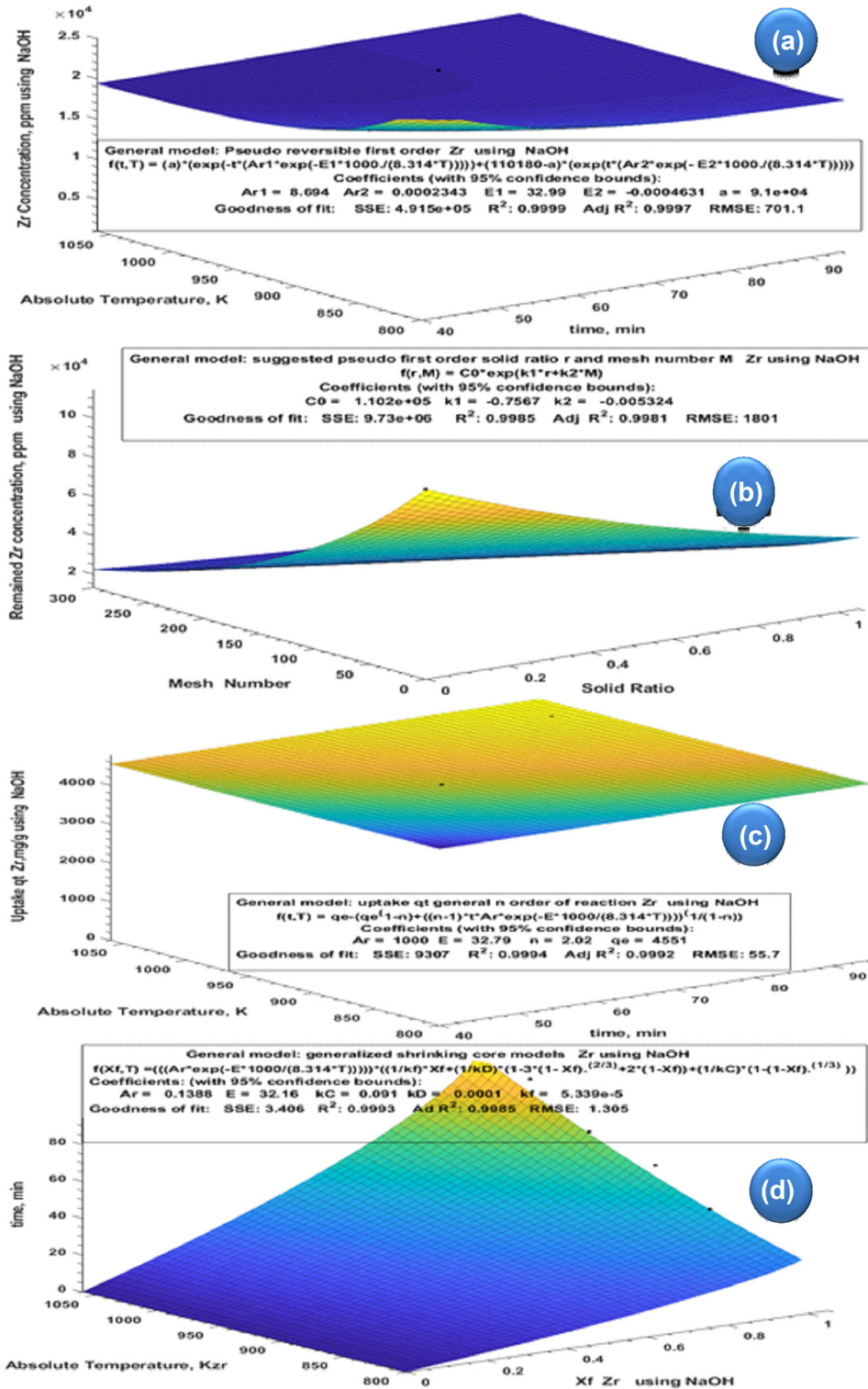


Fig. 4. (a, b) Suggested Pseudo reversible first order, (c) Uptake qt general and (d) Shrinking core model curves for Zr dissolution using sodium hydroxide.

By introducing the Arrhenius relationship (Eq. 2) in Eq. 9 and rearranging, we obtain:

$$(q_e - q_t)^{(1-n)} + q_e^{(1-n)} = (n - 1) t Ar \exp(\Delta E/RT) \tag{10}$$



**Table II. Activation energy for Zr, Ti, Nb and REEs dissolution processes using a pseudoreversible first-order model**

	NaOH-fusion			KOH-fusion		
	$E_1$ , kJ/mol	$E_2$ , kJ/mol	$R^2$	$E_1$ , kJ/mol	$E_2$ , kJ/mol	$R^2$
Zr	32.99	- 0.0005	0.999	31.55	-2.3e <sup>-14</sup>	0.997
Nb	37.67	1.027e <sup>-05</sup>	0.971	16.1	-0.0099	0.950
Ti	31.5	- 0.0032	0.991	31.35	0.03	0.994
REEs	32.1	-	0.993	32.35	-	0.985

$$q_e = q_e - \left[ q_e^{(1-n)} + ((n-1)t \text{ Ar exp}(\Delta E/RT)) \right]^{(1-(1-n))} \quad (11)$$

The uptake general model system was represented in 3D curves using MATLAB (Fig. 4c and S7C) (see supplementary data file). These figures simulated Eq. 11 and declared that, in a workable approximation, the uptake general model was the predominant kinetic model. This showed the uptake time relationship of this heterogeneous system in analogy to the pseudo-reversible first-order in a homogeneous system. The representation of nonlinear models in the 3D-enabled process allows the acquiring of many alternatives when facing any process shortage. In general, it is one of the good supports for taking a decision.

The activation energy presented in Table III gives information about the type of dissolution process using the two fluxes. These results matched well with the previous model results. The calculated correlation coefficients were closer to unity for the pseudo-first-order kinetic model. The calculated reaction order ( $n$ ) for the dissolution reactions of Zr, Nb, and Ti was closer to 2. On the other hand, for the REEs dissolution processes, the order of the reaction was one. The reaction order results agreed with the previous model results, and the fusion dissolution nature for Zr, Nb, and Ti through two reactions and one for REEs dissolution. The obtained data features in 3D Figs. 4c, and S7C (see supplementary data file), showing that the process could be approximated more satisfactorily by the uptake general model as the predominant mechanism.

### Shrinking Core Model

The mechanism proposed by the shrinking core model assumes the particles to be uniform non-porous grains. Initially, the reaction occurs in the grain surface and then the reaction zone moves into the solid leaving a product layer behind. The total radius of the particle remains constant, while the radius of the unreacted core and the layer of products vary over time as a function of conversion. The approximate solution of the shrinking core model applied in this work was a combination of the

**Table III. Activation energy for Zr, Ti, Nb, and REEs dissolution processes using the uptake general model**

	NaOH-fusion			KOH-fusion		
	$E$	$n$	$R^2$	$E$	$n$	$R^2$
Zr	32.79	2.02	0.999	31.95	1.95	0.998
Nb	37.7	2.02	0.992	16.99	1.845	0.981
Ti	32.1	1.95	0.997	31.75	1.95	0.997
REEs	32.47	1.03	0.996	32.1	1.03	0.994

resistances that can simultaneously occur in a particle under reaction: alkali diffusion in the layer surrounding the particle, alkali diffusion through the product layer around the unreacted core, and chemical reaction on the unreacted core surface. The graphical simulation that relates the conversion as a function of time ( $t$ ) for a spherical particle is given by:<sup>38</sup>

$$t = (1/K_f)X + (1/k_D) \left[ 1 - 3(1-X)^{2/3} + 2(1-X) \right] + (1/k_C) \left[ 1 - (1-X)^{1/3} \right] \quad (12)$$

where the terms  $K_f$ ,  $k_D$ , and  $k_C$  represent the resistances to the external mass transfer, product layer diffusion, and chemical reaction, respectively, and  $X$  is the fractional conversion.

By introducing the Arrhenius relationship (Eq. 2) into Eq. 12 and rearranging, we obtain:

$$f(X_f, T) = (\text{Ar exp}(-E 1000/RT)) \cdot (1/K_f) X + (1/k_D) \left[ 1 - 3(1-X)^{2/3} + 2(1-X) \right] + (1/k_C) \left[ 1 - (1-X)^{1/3} \right] \quad (13)$$

By applying the generalized shrinking core model (Eq. 13) on the dissolution process at several temperatures and times in 3D curves for Zr, Nb, Ti, and REEs, the experimental results were graphed using the MATLAB program as shown in

Figs. 4d and S7D (see supplementary data file). The activation energies,  $K_f$ ,  $k_D$ ,  $k_C$ , and correlation coefficients  $R^2$  for all the dissolution reaction experiments using the two alkalis are shown in Table IV. From the results, the activation energies of the dissolution processes for Zr, Nb, Ti, and REEs using the two fluxes were between 31 and 38 kJ/mole (except for the dissolution of Nb with KOH). The calculated correlation coefficients are closer to unity for the studied model. The obtained data features in 3D Figs. 4c and S7C (see supplementary data file) showing that the dissolution process was carried out through film diffusion control, which has the minimum value for all dissolution processes using the two fluxes ( $K_f < k_D < k_C$ ).

### Thermodynamic Characteristics

Using the fusion dissolution results under various temperatures ranging from 873 to 1023 K, the thermodynamic parameters of the studied fusion processes have been determined for Zr, Nb, Ti, and REEs using sodium and potassium hydroxides. These parameters were calculated for this system using the following non-linear Floatotherm (aniso-therm) and Van't Hoff equation. A Floatotherm term was suggested as a result of the temperature variation. Here, the Langmuir model was the starting point

for the Van't Hoff equation (Eq. 14):<sup>39</sup>

$$K_d = \exp(-\Delta H/RT) + (\Delta S/R) \quad (14)$$

and the Langmuir equation (Eq. 15):<sup>40</sup>

$$q = q_e KC/(1 + KC) \quad (15)$$

From these two equations, a suggested Floatotherm (aniso-therm) Van't Hoff equation (Eq. 16) was derived as follows:

$$f(C, T) = Q_m(\exp(-\Delta H/(RT) + \Delta S/R)) C^n / (1 + (\exp(-\Delta H/(RT) + S/R)) C)^m \quad (16)$$

where practically, n and m tend to unity. The suggested model can be represented in 3D using MATLAB as shown in Figs. S8–S11 (see supplementary data file), where  $K_d$  (ml/g),  $\Delta H$  (KJ/mol),  $\Delta S$  (J/mol.K),  $T$  (Kelvin), and  $R$  (KJ/K.mol) are the

distribution coefficient, the enthalpy, the entropy, the temperature in Kelvin, and the molar gas constant, respectively.

The Gibbs free energy,  $\Delta G$  (KJ/mol), is calculated from Eq. 17:<sup>41</sup>

$$\Delta G = \Delta H - T\Delta S \quad (17)$$

Dissolution enthalpy, entropy, Gibbs free energy, and the correlation coefficient for Zr, Nb, Ti, and REEs using sodium and potassium hydroxides have been plotted in Table S1 (see supplementary data file), the positive value of  $\Delta H$  confirming the endothermic nature of the dissolution process for the Zr, Nb, Ti, and REEs using sodium and potassium hydroxides. The negative value of the free energy of digestion,  $\Delta G$ , confirms the feasibility and spontaneous nature of the dissolution processes. Thus, the adsorption process was found to be endothermic and spontaneous. The  $\Delta S$  values had a negative value in most of the digestion experiments, indicating a decrease in the randomness at the solid/solution interface during the attack of the fused alkali on the ore particles.

### CONCLUSION

- XRF, XRD, and EDAX analysis proved that the Mylonite concentrate consisted mainly of Zr and Ti elements with considerable content from Nb, and REEs. Zircon, Titanite, Columbite, and Monazite were the main refractory minerals present in the concentrate of which the flux digestion was studied.
- Several batch tests were performed to optimize the Zr, Ti, Nb, and REEs dissolution by sodium and potassium hydroxides from the Mylonite concentrate of the Abu Rusheid area. Sodium hydroxide was more favorable than potassium hydroxide in dissolving Zr and Nb. On the other hand, potassium hydroxide was capable of dissolving Ti. Both alkalis achieved the goal of dissolving a maximum rare-earth content.
- Dissolution efficiencies of 83.4, 99.8, 69.7, and 97.1% for Zr, Nb, Ti, and REEs, respectively, were accomplished using sodium hydroxide with conditions of 1023 K, 90 min, 1:1.25 ratio, and 74  $\mu\text{m}$  ore particle size. Values of 79.5, 87.3, 90.5,

**Table IV. Activation energy for Zr, Ti, Nb, and REEs dissolution processes using the generalized shrinking core model**

	NaOH-Fusion					KOH-Fusion				
	E	K <sub>c</sub>	K <sub>D</sub>	K <sub>f</sub>	R <sup>2</sup>	E	K <sub>c</sub>	K <sub>D</sub>	K <sub>f</sub>	R <sup>2</sup>
Zr	32.16	0.091	0.0001	5.33e <sup>-5</sup>	0.999	31.15	0.1	0.001	3.97e <sup>-5</sup>	0.998
Nb	37.9	0.5	0.1	0.0012	0.992	16.08	0.5	0.31	1.75e <sup>-5</sup>	0.981
Ti	31.51	0.007	0.001	9.48e <sup>-6</sup>	0.991	31.47	0.007	0.006	6.82e <sup>-7</sup>	0.997
REEs	32.1	0.6	0.6	1.36e <sup>-5</sup>	0.996	32.98	0.099	0.034	8.95e <sup>-7</sup>	0.994

and 97.4% dissolution efficiencies for Zr, Nb, Ti, and REEs, respectively, were achieved using potassium hydroxide under 1023 K, 90 min, 1:1.75 ratio, and 44  $\mu\text{m}$  ore particle size conditions.

- Suggested pseudo-reversible first-order model, uptake general model, and shrinking core model fitted well with the experimental dissolution process results at several temperatures and times using group 1 experiments for Zr, Nb, Ti, and REEs using the two alkalis. Suggested pseudo-reversible first-order fitted well with the experimental dissolution process results using group 2 experiments.
- Using the three models, the activation energies of the dissolution processes had converging results ranging between the 31 and 38 kJ/mole for Nb, Zr, Ti, and REEs using the two fluxes (except for the dissolution of Nb with KOH). All of the dissolution processes using the two fluxes were carried out through two reactions (parallel or reversible), except for the dissolution of the REEs. The dissolution processes were carried out through film diffusion control which had the minimum value for all the dissolution processes.
- The thermodynamics calculations showed the endothermic nature of the dissolution processes for the Nb, Zr, Ti, and REEs using sodium and potassium hydroxides, and the feasibility and spontaneous nature of the dissolution processes with a decrease in the randomness at the solid/solution interface during the attack of the fused alkali on the ore particles.

### CONFLICT OF INTEREST

On behalf of all the authors, the corresponding author states that there is no conflict of interest.

### SUPPLEMENTARY INFORMATION

The online version contains supplementary material available at <https://doi.org/10.1007/s11837-021-04837-1>.

### REFERENCES

1. M.A. Ali, *Geologija* 55, 1. (2012).
2. M.E. Ibrahim, G.M. Saleh, T. Amer, F.O. Mahmoud, A.A. Abu El Hassan, I.H. Ibrahim, M.A. Aly, M.S. Azab, M.A. Rashed, F.M. Khaleal, and M.A. Mahmoud, *Internal report* (Nuclear Materials Authority, Cairo, 2004).
3. M.E. Ibrahim, A.A. Abd-El-Wahed, F. Oraby, Abu El-Hassan, M.M. EL GaLy, and K. Watanabe, *The Fifth International Conference on the Geology of Africa*, Assiut-Egypt, 1 (2007).
4. M.A. Ali, D.R. Lentz, and D.C. Hall, *Chin. J. Geochem.* 30, 226. (2011).
5. A.H. El-Afandy, M.G. El-Feky, S. Taha, S.M. El Minyawi, and H.A. Sallam, *Greener J. Geolog. Earth Sci.* 4, 3. (2016).
6. M.E. Ibrahim, M.M. El Tokhi, G.M. Saleh, and M.A. Rashed, *7th Intern* (Conf. on Geochem. Fac. Sci. Alex. Univ. Alex, Egypt, 2006).
7. G.M. Saleh, *Chinese J. Geochem.* 26, 333. (2007).
8. M.E. Ibrahim, K. Watanabe, G.M. Saleh, and W.S. Ibrahim, *Arabian. J. Geosci.* 8, 9261. (2015).
9. D.I. Zaki, N. Shawky, E.M. El-Sheikh, F.Y. Ahmed, and M.E. Ibrahim, *Chinese J. Geochem.* 31, 64. (2012).
10. M.M. Fawzy, M.S. Kamar, and G.M. Saleh, *Inter. Rev. App. Sci. Eng.* 12, 134. (2021).
11. Y.M. Khawassek, A.A. Eliwa, E.A. Gawad, and S.M. Abdo, *J. Rad. Res. Appl. Sci.* 8, 583. (2015).
12. O.M. El-Hussaini, and M. Mahdy, *Hydrometallurgy* 64, 219. (2002).
13. Y. Xiuli, Z. Junwei, F. Xihui, and Q. Tingsheng, *J. Refract. Met. Hard Mater.*, 45 (2014).
14. A.B. Eduardo, and J.M. Francisco, *Miner. Eng.* 21, 2. (2008).
15. Z. Bo, L. Chengjun, L. Chunlong, and J. Maofa, *Miner. Eng.* 65, 17. (2014).
16. P. Cameron, and M. Gavin, *Ore Geol. Rev.* 107, 629. (2019).
17. S.A. Farzaneh, N. Mohammad, and G. Ahmad, *J. Rare Earths* 35, 8. (2017).
18. R.C. Doman, and A.M. Alper, *Refractory minerals* (Springer, Boston, 1983).
19. J.F. Reginaldo, J.B.D. Achilles, and C.A. Julio, *Hydrometallurgy* 117–118, 93. (2012).
20. W. Xiaohui, Z. Shili, X. Hongbin, and Z. Yi, *Hydrometallurgy* 98, 219. (2009).
21. X. Tianyan, W. Lina, Q. Tao, C. Jinglong, Q. Jingkui, and L. Changhou, *Hydrometallurgy* 95, 22. (2009).
22. F. Habashi, *Extractive metallurgy of rare earths. Can. Metall. Q.* 52, 224. (2013).
23. G.M.A. Wahab, W.M. Abdellah, A.M. Yousif, and A.E. Mu-bark, *Mining Metall. Explor.* 2019, 1. (2019).
24. H. Zhou, S. Zheng, and Y. Zhang, *Chin. J. Proc. Eng.* 3, 2712. (2003).
25. E. Abdelgawad, *J. Basic Envir. Sci.*, 7, (2020).
26. M.A. Suélen, D.D. Michele, L.P.D. Tirzhá, J.J. Humberto, and F.P.M.M. Regina, *Chem. Eng. J.* 283, 388. (2016).
27. S. Nagar, *Introduction to MATLAB for Engineers and Scientists: Solutions for Numerical Computation and Modeling* (Apress, New York, 2017).
28. G. Oehlert, *A first course in design and analysis of experiments* (Freeman, New York, 2010).
29. S. Parirenyatwa, L. Escudero-Castejon, S. Sanchez-Segado, Y. Hara, and A. Jha, *Hydrometallurgy* 165, 213. (2016).
30. A.J. Manhique, W.W. Focke, and C. Madivate, *Hydrometallurgy* 109, 230. (2011).
31. R. Subagja, and A. Royani, *Mater. Sci. Eng.* 541, 1. (2019).
32. Y. Aristanti, Y.I. Supriyatna, N.P. Masduki, and S. Soepriyanto, *Mater. Sci. Eng.* 285, 1. (2018).
33. X. Wang, S. Zheng, H. Xu, and Y. Zhang, *Hydrometallurgy* 98, 219. (2009).
34. R.J.F. da Silva, A.J.B. Dutra, and J.C. Afonso, *Hydrometallurgy* 117, 93. (2012).
35. N.A. Mohammed, and A.M. Daher, *Hydrometallurgy* 65, 103. (2002).
36. I. Tinoco, and W.S. Wang, *Physical chemistry: principles and applications in biological sciences*, 3rd edn. (Prentice Hall, Berkeley, 1995).
37. K. Connors, *Chemical Kinetics: The Study of Reaction Rates in Solution* (VCH, New York, 1990).
38. E. Abdelgawad, *Nucl. Sci. Scie. J.*, 8 (2019).
39. P. Atkins, and J. de Paula, *Physical Chemistry*, 8th edn. (Freeman, New York, 2006).
40. K.Y. Foo, and B.H. Hameed, *Chem. Eng. J.* 156, 2. (2010).
41. P. Perrot, *A to Z of Thermodynamics* (Oxford University Press, New York, 1998).

**Publisher's Note** Springer Nature remains neutral with regard to jurisdictional claims in published maps and institutional affiliations.